PAPER

Experimental study of gliding arc plasma channel motion: buoyancy and gas flow phenomena under normal and hypergravity conditions

To cite this article: Lucia Potoáková *et al* 2017 *Plasma Sources Sci. Technol.* **26** 045014

View the article online for updates and enhancements.

Related content

- Gravity effects on a gliding arc in four noble gases: from normal to hypergravity
  L Potoáková, J Šperka, P Zikán et al.

- Dynamics, OH distributions and UV emission of a gliding arc at various flow-rates investigated by optical measurements
  Jiajian Zhu, Zhiwei Sun, Zhongshan Li et al.

- A 2D model for a gliding arc discharge
  St Kolev and A Bogaerts

Recent citations

- OH and O radicals production in atmospheric pressure air/Ar/H_2O gliding arc discharge plasma jet
  N C ROY *et al*

Experimental study of gliding arc plasma channel motion: buoyancy and gas flow phenomena under normal and hypergravity conditions

Lucia Potočňáková[1], **Jiří Šperka**[1,2], **Petr Zikán**[1], **Jack J W A van Loon**[3,4], **Job Beckers**[5] **and Vít Kudrle**[1]

[1] Department of Physical Electronics, Masaryk University, Kotlářská 2, 61137 Brno, Czechia
[2] Czech Metrology Institute, Okružní 31, 638 00 Brno, Czechia
[3] DESC (Dutch Experiment Support Center), Department of Oral and Maxillofacial Surgery/Oral Pathology, VU University Medical Center & Academic Centre for Dentistry Amsterdam (ACTA), Amsterdam, The Netherlands
[4] European Space Agency (ESA), ESTEC, TEC-MMG, Noordwijk, The Netherlands
[5] Faculty of Applied Physics, Eindhoven University of Technology, PO Box 513, 5600 MB Eindhoven, The Netherlands

E-mail: nanai@mail.muni.cz

Abstract

The details of plasma channel motion are investigated by frame-by-frame image analysis of high speed recording of a gliding arc. The gliding arc is operated in several noble gases at various flow rates, voltages and artificial gravity levels. Several peculiarities in evolution of individual glides are observed, described and discussed, such as accelerating motion of plasma channel or shortcutting events of various kinds. Statistics of averaged parameters are significantly different for buoyancy and gas drag dominated regimes, which is put into relation with differing flow patterns for hypergravity and high gas flow.

Keywords: gliding arc, hypergravity, gas drag, buoyancy, flow dynamics, atmospheric pressure plasma, centrifuge

(Some figures may appear in colour only in the online journal)

1. Introduction

The electric arc is one of the oldest known plasma discharges [1]. One of its typical features is the intensively ohmically heated plasma channel. Consequently, a gravity-dependent buoyant force arises, originating from the temperature and density difference between the hot discharge channel and its surrounding colder atmosphere. Buoyancy lifts the plasma channel which then assumes a typical arc-like curved shape between two fixed points. The arc is a typical example of a thermal plasma [2], with gas and ion temperature as high as electron temperature. While the plasma chemistry of the arc can be successfully employed in many industrial applications [3], it is its high temperature that typically governs its use [4].

However, if certain conditions are met, the plasma at atmospheric pressure does not thermalise and cold non-thermal plasma [5] with hot electrons yet relatively cold neutral species can be produced—the atmospheric pressure glow discharge (APGD) [6, 7]. Such discharge is fundamentally different from the arc discharge in many essential characteristics: besides having a low temperature of heavy species it has also a lower conductivity, a lower ionisation degree and it is usually diffuse. The APGD resembles its well known low pressure counterpart even in appearance [8], including the

typical distribution of dark and luminous spaces [9]. The APGD operates in various gases [9, 10], among them the noble gases, nitrogen, oxygen and air being the most studied. However, at higher pressures the instabilities in the cathode region and thermalisation of the discharge column often lead to a generally undesirable glow-to-arc transition. Various ways to prevent the discharge from the glow-to-arc transition have been proposed and successfully tested. Examples are cooling the electrodes by water [11], scaling the discharge down to microplasma dimensions [12], adding at least one insulating layer between the electrodes (DBD configuration) [13, 14], using microhollow cathode as a source of electrons [15] or operating at flow rates high enough to cool the discharge [16]. Current limited point-to-point atmospheric pressure discharges were operated with both gas flow longitudinal [17] and transverse [18] in respect with the plasma channel. If the transverse gas drag is strong enough, the discharge will start to resemble the gliding arc discharge, with prolonging plasma column and periodical reignitions [16].

The actual gliding arc discharge [19] is produced similarly, but in the discharge electrodes geometries and configurations (typically slanted/divergent), which enables the plasma channel, including its anchor points, to slide along the electrodes. In gliding arc, the plasma channel is ignited in the shortest path in-between the electrodes, where the electric field is the strongest and then it is moved by two forces: (i) the buoyant force and/or (ii) the gas drag. Typically, the device is oriented in such way, that both of these forces act upwards. In the common configuration, due to a divergent shape of the electrodes, the higher the channel ascends, the longer it gets, until it quenches at the moment when the power of the source is not sufficient to sustain the discharge anymore [20, 21]. Consequently, a new plasma channel ignites at the shortest electrode distance. This cycle, repeating in a quasi-periodic manner with characteristic time period and gliding (repetition) frequency, is one of the gliding arc most distinguishing features. Using the parameters averaged over many cycles, the gliding arc can be described sufficiently, even though the discharge can be considered chaotic at shorter time scales and individual glides can differ a lot due to unpredictable microdynamics of the discharge [22] (e.g. breakdown phenomena, discrete points of gliding arc connection to electrodes, local sputtering effects, shortcutting events, hysteresis, turbulent flow effects etc).

Although the name gliding arc suggests that the gliding arc plasma is in thermal equilibrium, just as the typical arc is, it can also be (and often is) strongly non-equilibrium and more similar to non-thermal APGD. The question of thermal (non) equilibrium in gliding arc discharge can be even more complicated, as the discharge can consecutively change its properties during one glide [23], from the ones nearly identical to a standard thermal arc at short channel lengths, to a cold plasma at longer discharge channels. In both experimental and theoretical studies, a lot of attention was paid to proper identification of gliding discharge regime and to comparison of arc and glow modes [24]. Another widely researched topic concerning gliding arc are its electrical properties [25, 26], the movement and characteristics of the

anchor points to the electrodes [27, 28], spectroscopy studies [29], electrode geometry [30] and others [31, 32]. From the application point of view, gliding arc is closely related to the established protective devices against voltage surges, such as circuit breakers and lightning arresters. In the current research though, more attention is paid to gliding arc plasma chemistry [33], enabling for example gas conversion and decontamination [34, 35].

However, as the applications of gliding arc usually require its operation in a flow regime and the gas flow rates tend to be relatively high (up to many tens of slm—standard litres per minute), most of the studies have been carried out at high flow rates. Even the studies [22, 36] concentrating on the flow rate influence chose the lowest rate of as much as several slm. As a result, the majority of these studies neglect the influence of buoyant forces at all, as at such conditions the gas flow governs the discharge dynamics. The upwards motion of plasma channel is then mostly caused by gas drag. Turbulent conditions, associated with high flow rate, perturb the plasma channel evolution in rather chaotic way. The subtle effects of buoyancy, plasma particles diffusion or even self-induced electromagnetic forces are difficult to observe in such regimes and thus were out of research focus.

Recently, we performed several experiments [37–40] with gliding arc discharge at the centrifuge, which simulated the hypergravity conditions up to $18g$ and thus allowed us to study gliding arc in buoyancy dominated regime. The first results proved the strong influence of increased gravity on the plasma channel, such as higher frequency of gliding and lower maximum height reached by plasma. This paper aims to contribute to the deeper understanding of the complex behaviour of gliding arc discharge by a detailed study of the plasma channel motion. This is achieved not only through averaged macroscopic parameters, but also by accentuating the instantaneous dynamics of individual plasma channel evolution during one glide and by comparing the results under hypergravity conditions with the high flow rate conditions and other parameters.

2. Experimental

2.1. GRAVARC apparatus

Custom made gliding arc setup 'GRAVARC' (GRAVity ARC) was specially constructed for operation under hypergravity conditions ($1g$–$18g$) [41] in the Large Diameter Centrifuge (LDC) of ESA/ESTEC (European Space Research and Technology Centre of European Space Agency, Noordwijk, the Netherlands). Full details of the experimental setup are described in [38], including the pre-requisitions for hypergravity experimentation at the centrifuge. Here, only a brief description of the experimental setup follows.

In figure 1, the discharge chamber is schematically visualised from the front view, including its dimensions. The front and back walls of the discharge chamber were made from heat resistant glass to enable direct visual observation of the discharge using digital cameras. For standard photographs, cameras Canon Power Shot A460 and Nikon D3100 were used, and for
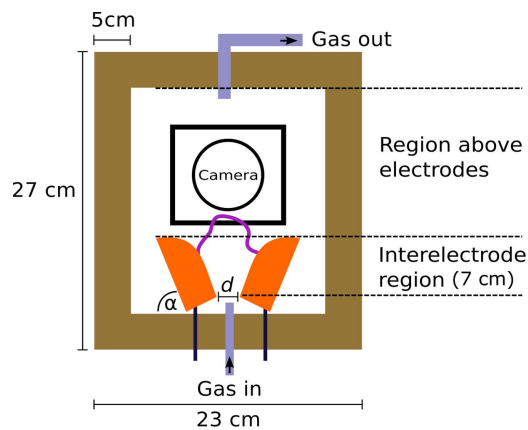
Figure 1. Schematic drawing of the discharge chamber, front view, $d = 4.5$ mm and $\alpha = 72°$.

high speed videos, the Casio EX-ZR100. The video recording speed was 1000 frames per second (occasionally only 480 fps), which was sufficient for the gliding speeds observed. The gas was fed into the discharge chamber from the gas bottles via fused silica tube (3 mm inner diameter) passing through the bottom of the nonconductive discharge chamber, centred in-between the electrodes. Four noble gases (^{4}He, ^{20}Ne, ^{40}Ar and ^{84}Kr) were chosen as working gases for this study, as their atomic masses (which affect also dependent quantities, e.g. thermal conductivity) cover a wide range, yet they, as monoatomic non-reactive gases, are similar in other properties. The gas flow rate was regulated by the calibrated needle valves and generally was kept rather low. Typical values of the gas flow rate ranged from tens of sccm (standard cubic centimetre per minute) up to more than one slm (standard litre per minute) and corresponding flow speeds at the end of tube nozzle from tenths of m s^{-1} up to more than 2 m s^{-1}. However, the flow speeds at higher positions in the discharge chamber were significantly lower due to flow expansion. Opposite to the gas input, another fused silica tube functioned as the gas exhaust. Before the release to the ambient, the exhaust gas passed through a long tubing which prevented any back-streaming of outer air into the chamber.

Copper discharge electrodes were placed near the bottom of the chamber. The minimum distance between them was fixed at value of $d = 4.5$ mm and the angle α (see figure 1) at value of 72°. The highest point of electrodes virtually divides the discharge chamber into two sections: (i) interelectrode region (up to 7 cm above the minimum distance position) and (ii) the region above the electrodes. The border between these two regions is marked by a grey dashed horizontal line in the following figures, where appropriate.

The discharge's power supply consisted of a variable autotransformer (variac) and an inductance leakage type high-voltage (HV) transformer with inherent current limitation. The variable autotransformer input was a standard AC electric power (230 V, 50 Hz). Its output (0%–100% of input) was applied to primary winding of HV transformer. Secondary winding of HV transformer was directly connected to discharge electrodes. Open circuit transformation ratio of HV

transformer was 1:40. In such way, the suitable working power to the gliding arc discharge could be set, with maximum available high voltage of 10 kV. Electrical parameters were measured both at (i) high voltage part of the circuit by an oscilloscope with high voltage probe and current probe and (ii) low voltage part on the primary winding of the high voltage transformer, where the effective voltage, current and power were recorded by digital multimeters connected to PC.

2.2. Operating parameters

In this paper, the gliding arc is studied under a wide range of conditions (gravity level, gas flow rate, voltage and working gas). Operation in four different noble gases made the choice of experimental parameters (especially the gas flow) rather unstraightforward, as for achieving qualitatively the same discharge regime in various gases, quantitatively different experimental conditions had to be set. It was previously shown [37] that substantially higher gas flow is needed to maintain the gliding motion of plasma channel in helium (as the lightest of noble gases), especially at 1*g*. At higher gravity, increased *g*-force can induce the gliding even under flow conditions resulting in a stable arc at 1*g*. The setting of the helium gas flow rate has always been subject to these peculiarities and because of this the helium gas flow rate is always higher than the gas flow rate of other gases used in this work. The same goes for the voltage, which has also been kept higher for the discharge in helium.

The rms value of the voltage on the primary winding of HV transformer (primary voltage) was chosen as the suitable parameter for further discussions, as it was controlled directly and kept constant during individual experiments, while the actual instantaneous voltage on the electrodes (and also instantaneous power consumed) varied during each glide, as can be seen in figure 2(c).

2.3. Data processing

The main motivation of this work is to determine the various mechanisms beyond the gliding arc periodic movement. For this, the high speed video (480 or 1000 frames per second) and long exposure (up to several seconds) photography were employed. The video recordings were processed frame by frame to trace several parameters describing the gliding arc movement. A typical result of image processing of one full glide of discharge in argon can be seen in figure 2(a). The image in figure 2(b), composed of several video frames, illustrates some of the measured quantities. These are:

- minimum bottom (b_{min})—the place of gliding arc ignition at minimum interelectrode distance,
- instantaneous top (h)—the vertical distance between the minimum bottom and the highest point reached by plasma channel in the given frame,
- maximum reached height (h_{max})—the vertical distance between the minimum bottom and the highest point reached by plasma in one full glide, before new ignition,
- instantaneous bottom (b)—the vertical distance between the minimum bottom and the lowest point of discharge
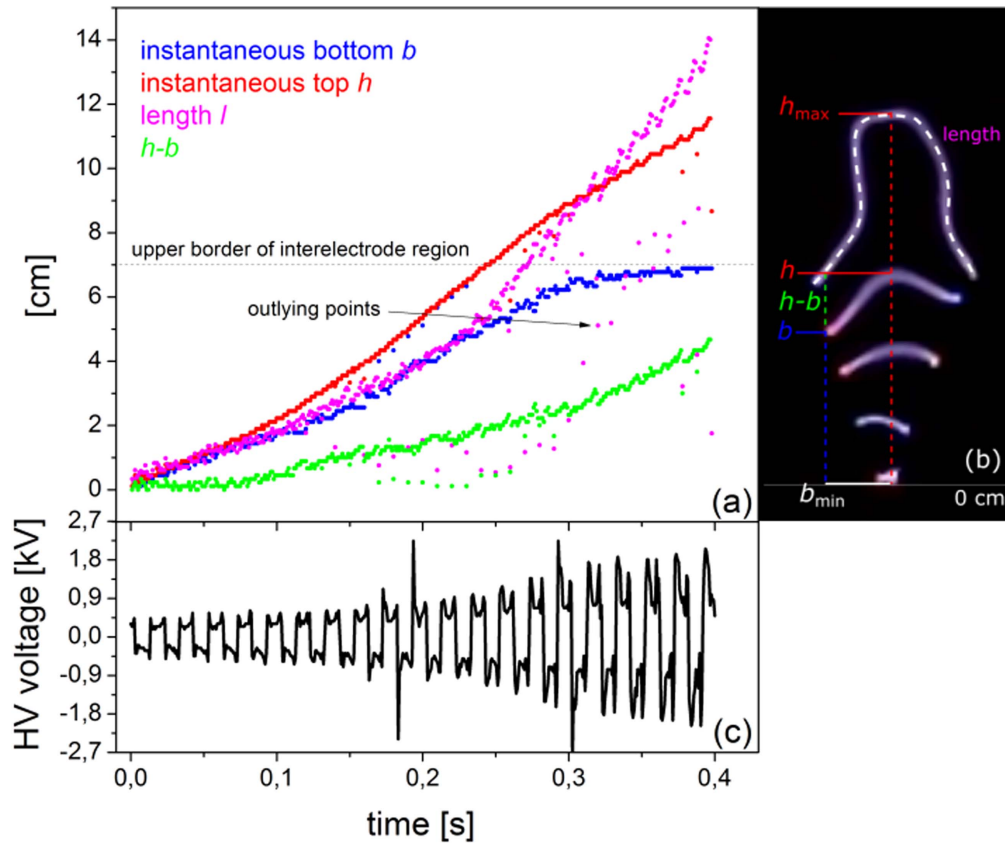
Figure 2. Various characteristics of one full discharge channel glide. (a) Results of video frame sequence processing including the outlying points (grey dashed line marks the upper border of the interelectrode region) (b) several video frames combined together to explain the meaning of measured parameters, (c) oscillogram of instantaneous high voltage between the electrodes.

channel, which is in the majority of the cases one of the plasma-electrode contact spots,

- h–b—the difference between instantaneous top and instantaneous bottom,
- discharge channel length l—the geometric length of the discharge channel in the given frame,
- one glide period—the time between the two successive ignitions (it is effectively equivalent to a time difference between the ignition at b_{min} and disruption of the plasma channel at maximum elongation, because the new ignition usually follows after the disruption without any or minimal delay),
- gliding frequency—reciprocal value of average glide period.

The processing of the frames was done in Mathematica [42]. The programme worked with the set of large number of consequent high speed video frames. Firstly, it converted each video frame into black and white, then thinned the image of single plasma channel captured in the frame into 1px wide curve that was easy to work with and through various basic mathematic functions, the programme determined all the parameters listed above. The outlying points visible in figure 2(a) usually originate from the frames when the instantaneous voltage (50 Hz AC) was near zero and so the discharge was too dark to be correctly evaluated by the programme. These outliers can be eliminated from further data

processing and will not be presented in further graphs. However, as the length l is the parameter most prone to this kind of processing error, the focus was preferentially on more robust parameters, such as the instantaneous top or instantaneous bottom. Most of the parameters listed above describe instantaneous position of plasma channel, evolve during each glide and their evolution varies between the glides. This kind of parameter was not averaged and when presented, an exemplary glide was hand-picked to best represent the discharge typical behaviour. On the other hand, the average maximum height and the gliding frequency were always calculated as an average value from at least ten (up to more than hundred) individual glides.

3. Results

3.1. Evolution of the plasma channel during one glide period

The gliding arc discharge is typical by its quasi-periodic evolution, igniting at the point of narrowest distance in-between the electrodes, followed by the upwards movement of the hot plasma channel and finishing by its disruption at the maximum reachable length and immediate reignition back at the minimum interelectrode distance [19]. There are two main forces governing the upwards movement of the plasma channel: (i) the effective buoyant force $F_b = V \cdot (\rho_{gas} - \rho_{plasma}) \cdot g$ and/or
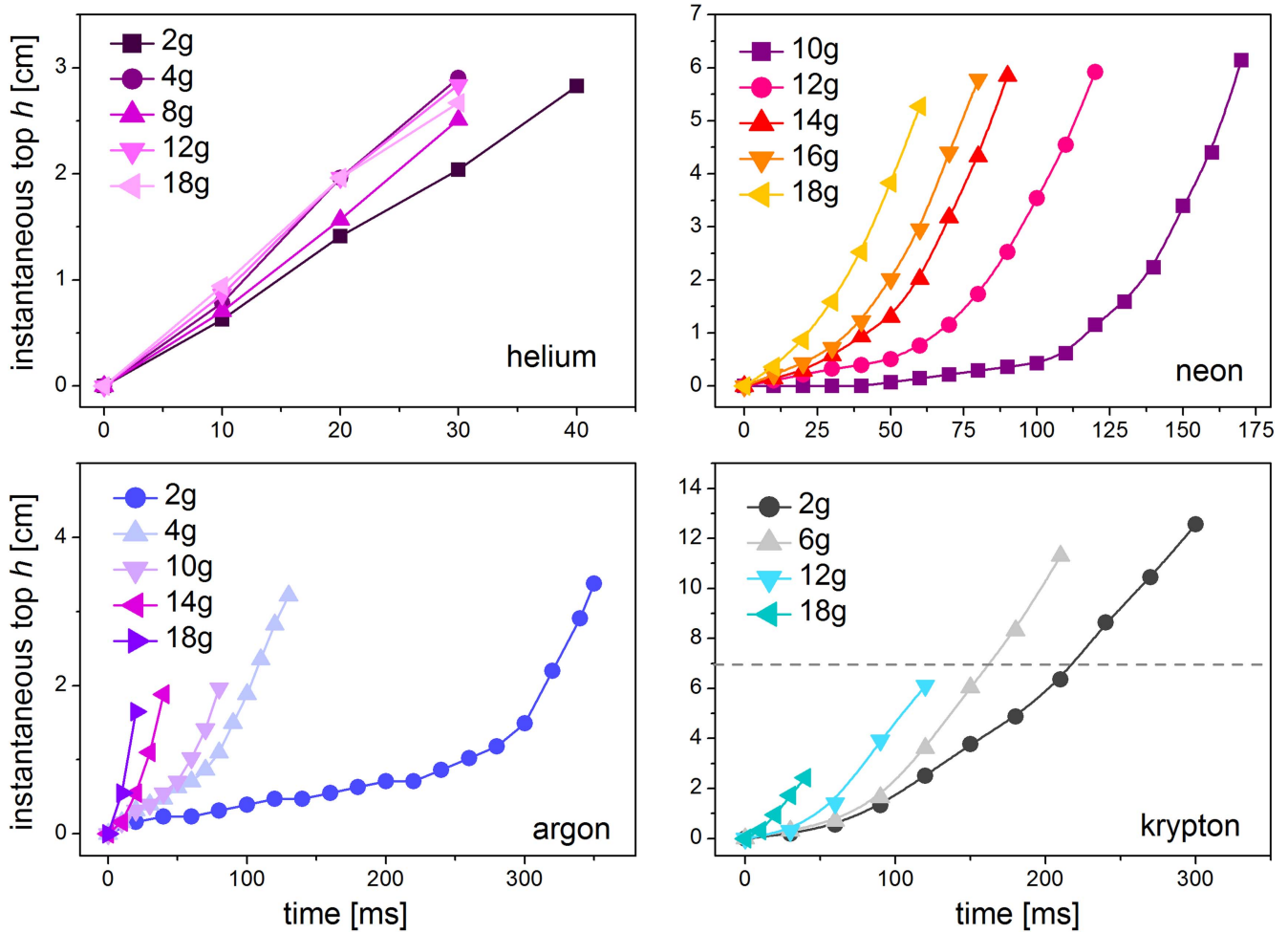
Figure 3. Evolution of the instantaneous top *h* during one full glide for various *g*-levels for gliding arc in four noble gases at various flow rates and voltages (He: 650 sccm, 200 V, Ne: 150 sccm, 100 V, Ar: 150 sccm, 100 V, Kr: 400 sccm, 100 V). Grey dashed line in Kr graph marks the upper border of the interelectrode region.

(ii) the gas drag $F_\mathrm{d} = 1/2 \cdot \rho_\mathrm{gas} \cdot v^2 \cdot C_\mathrm{d} \cdot A \cdot v/|v|$, where *V* and ρ_plasma are the volume and the mass density of plasma channel, ρ_gas is the mass density of the surrounding gas, *g* is gravitational acceleration on the surface of Earth, *v* is the speed of the plasma channel relative to the surrounding gas, C_d is the drag coefficient and *A* is the cross-sectional area. The term $v/|v|$ characterises the orientation of the drag force, which can either accelerate or decelerate the plasma channel, depending on actual conditions. The difference of mass densities is directly proportional to temperature differences. While the surrounding atmosphere remains near room temperature (300 K), the plasma channel temperature can be estimated, based on the reports of other authors working with similar conditions [6, 8, 24, 26, 29], to be around 1000–1500 K.

The details of the gliding arc evolution are to a great extent governed by unpredictable and always changing deviations from stability, often induced by local flow turbulences, thermal effects, local roughness of electrodes and self induced electromagnetic forces. As a result, individual glide periods may vary, yet in most of the cases it is possible to find an 'average' or typical glide.

In the sets of graphs in figures 3 and 4, the examples of evolution of instantaneous top *h* in one gliding period—from ignition until quenching—can be seen, either for various *g*-gravity levels (figure 3), or various primary voltages (figure 4). Each graph corresponds to one gas (colour coded for easier orientation) and shows a typical full glide for each various gravity or voltage. The situation in helium is different from the other three gases, as the gas flow rate needed for helium to glide was the highest. In this experiment, the gravity induced changes underwent by the gliding arc in helium were then rather low to be conclusively identified.

The hypergravity results (figure 3) for the heavier gases are similar to each other. The plasma channel upwards movement always speeded up with increasing *g*-level. Moreover, the graphs show that the speed of plasma channel movement under hypergravity is generally not linearly dependent on time, but has rather a two-phase character (most pronounced in neon). The movement in the first phase, in lower positions of plasma channel, seems to be reluctant and as the arc gets to higher positions (second phase), it accelerates. The different time needed for the arc to reach the maximum top height is then mostly dependent on the duration
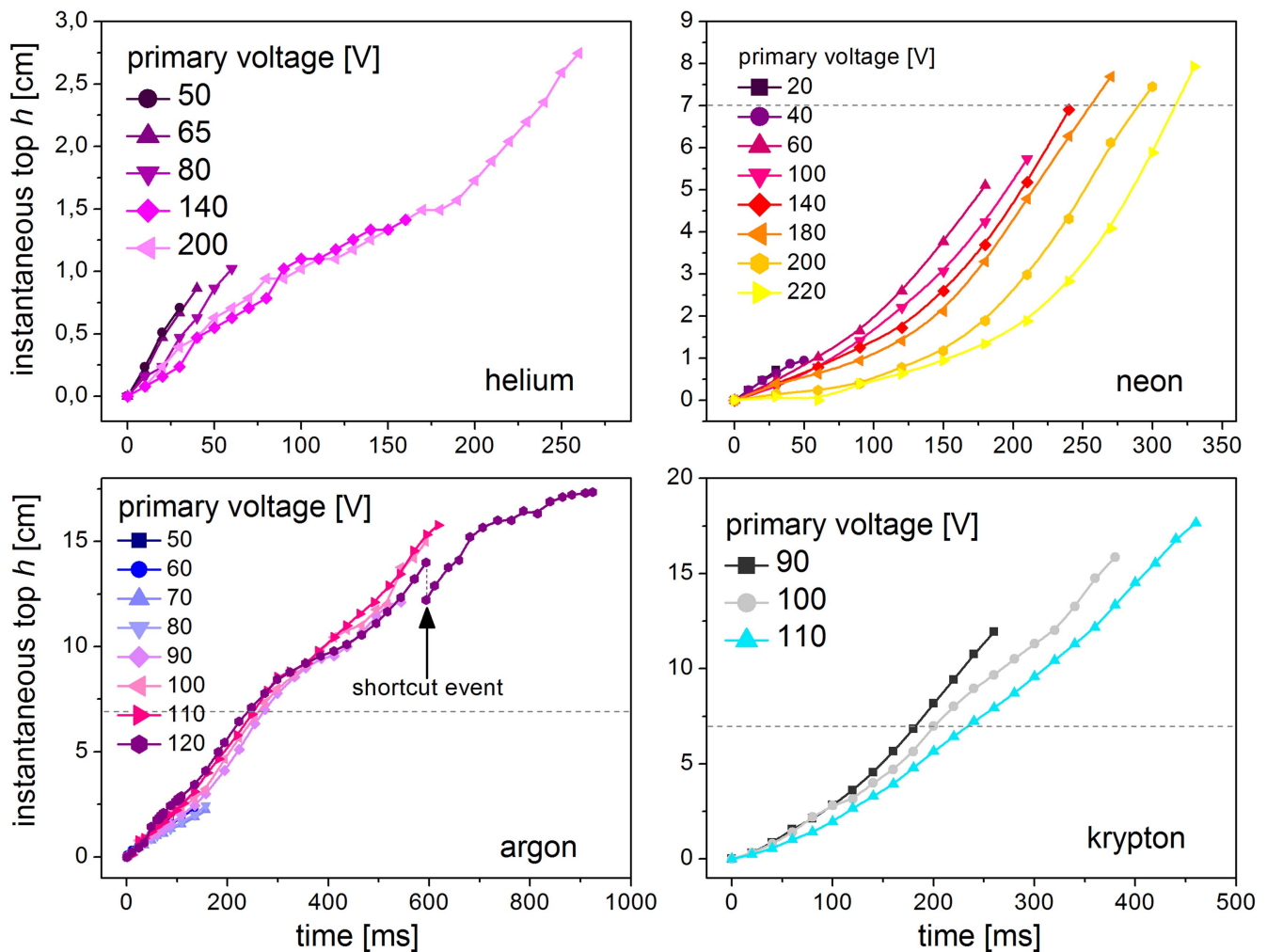
Figure 4. Evolution of the instantaneous top *h* during one full glide for various primary voltages for gliding arc in four noble gases at various flow rates (He: 1400 sccm, Ne: 400 sccm, Ar: 400 sccm, Kr: 400 sccm) and 1*g* gravity level. The voltage range, from actual ignition voltage up to the highest voltage limited either by the power supply or the parameters of the discharge chamber, is different for each gas. Grey dashed line in Ne, Ar and Kr graphs marks the upper border of the interelectrode region.

of slow motion phase. It might be tempting to attribute the two phase character to the plasma channel reaching the top of the electrodes and ascending above them, but the heights at which the acceleration of the plasma channel takes place are too low which excludes this explanation.

The two-phase character is still present for some gases also under normal, 1*g* gravity (see figure 4), again best visible for neon, although the first phase is not so flat as in hypergavity conditions and thus the two phases are less discerned. Surprisingly, it seems that the higher the primary voltage, the slower the movement of the plasma channel. This is probably caused by the subtle effects of channel reignition, explained in following paragraphs.

Due to AC 50 Hz operation, the discharge periodically extinguishes (or almost extinguishes) when instantaneous voltage comes close to zero and then reignites again. This off-time between extinction and reignition usually lasts around 0.5 ms which is several orders longer than the recombination time estimation (hundreds of nanoseconds). However, even then the remaining ionisation is still present and substantially higher than the natural ionisation degree. From the point of

view of plasma reactions it might be negligible but it has tremendous influence on the breakdown of the new plasma channel [43–45].

The next plasma channel reignites in the most favourable position, i.e. where the rising voltage (after zero crossing) on electrodes reaches the breakdown threshold first. This breakdown voltage depends on the vertical position not only due to angled electrodes, but also due to a local residual ionisation, which depends on the system history. The highest preionisation is directly in the wake of the last plasma channel which spreads due to the diffusion omnidirectionally but also rises upwards due to the gas drag and thermal buoyancy. At high enough current densities (reached for high primary voltages), there are so many excited and ionised particles produced, that residual ionisation is sufficiently high even above or below the current wake position. In that case the next reignition can occur below the current wake position due to higher electric field in narrower gap. So while the new channel generally tends to reignite in the moving wake of the previous channel, at sufficiently high residual ionisation it may prefer the path at lower vertical position where the
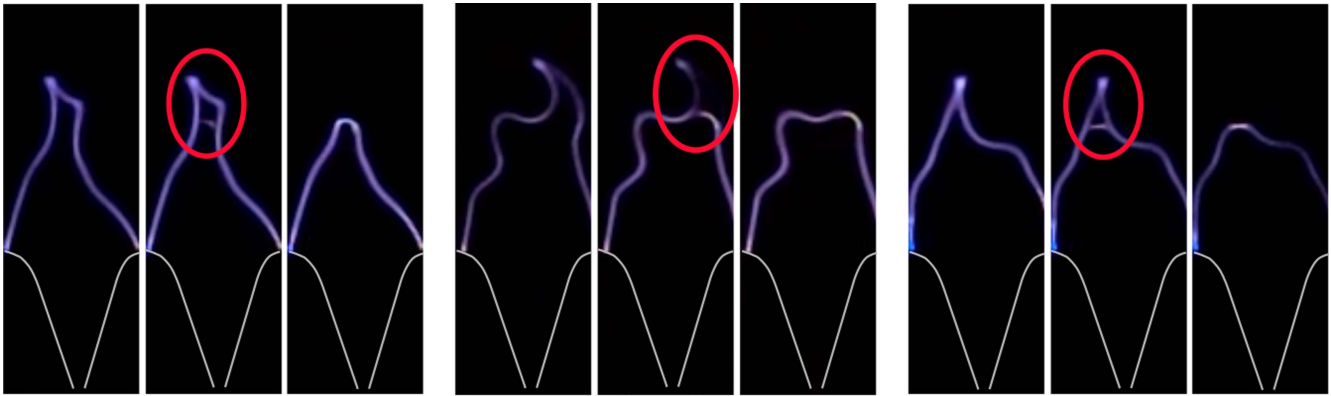
Figure 5. Three independent examples of shortcut events above electrodes. The time delay between successive video frames is 1 ms. Experimental conditions: argon, 400 sccm, 120 V primary voltage, 1*g*.

breakdown voltage is lower. Effectively, this can reduce the observed upward speed of the gliding arc. This slowed down motion continues, until the growing concentration of accumulating active particles in upper region overcomes the electric field advantage of the lower position and the transition to faster movement occurs.

Related to this, there could be also another mechanism, for which the maximum height reached in the previous glide period is essential. At stable experimental conditions it is likely that one glide was preceded by a very similar one. In figures 3 and 4 it can be seen that for higher voltage/lower *g*-level, the initial slow motion phase lasted longer and the gliding arc ascended to higher h_{max}. With higher h_{max}, longer period of gliding (lower gliding frequency) is associated. Thus, the excited or ionised particles that remained lingering in lower region had more time for recombination before the discharge reignites in low position again, than in the case where the discharge resided in the low positions for all the time. In the latter case, the movement is from the start faster, because the plasma channel might benefit from high pre-ionisation since the very beginning of its development.

Figure 4 reveals another interesting feature. In graph for discharge in argon, at highest voltage, the growth of instantaneous top is interrupted by a sudden fall. The decrease in instantaneous top happened after a new, shorter discharge path was formed. This shortcut event has been observed also by other authors [22]. Several examples of shortcutting events captured at successive video frames can be seen in figure 5. All three presented shortcuts happened above the interelectrode region, when the discharge reached near-maximum height. The newly formed section of the plasma channel is slightly brighter than rest of the plasma channel, but shortly after full disappearance of the old pathway the light emission intensity equalises again. The shortcut events above electrodes were observed to occur at any phase of sine voltage supply, i.e. not only during the zero-crossing.

Yet another situation, not visible at previous figures, is demonstrated in figure 6—at higher gas flows the shortcut events can appear even in the interelectrode space. In figure 6(a), the evolution of gliding arc plasma channel in relatively low gas flow conditions (280 sccm) is shown. It can be seen, that in this case, the position of instantaneous top is

linearly dependent on time throughout the whole glide and gliding motion is continuous, until its quenching at maximum height. The speed is constant at value of $0.25\,\mathrm{m\,s}^{-1}$.

The situation significantly changes when increasing the gas flow rate to a higher value (1000 sccm), as is seen in figure 6(b). If the detailed evolution depicted by red symbols was ignored and the attention was only paid to the starting and ending points (linear blue line), the increase in linear speed ($0.39\,\mathrm{m\,s}^{-1}$ would still be observed, just as expected [22, 37] for an increased flow rate. However, in reality, the upwards motion of the plasma channel is disrupted by several drops in height and the piece-wise average speed (green colour in figure 6(b)) of the plasma channel in each segment of the evolution is higher than the overall linear approximation of the average speed. As the microdynamics of the plasma channel is governed by this higher, actual speed, the macroscopic approach might in some cases lead to inaccurate conclusions.

The visual examples of interelectrode shortcut events can be found in figure 7. The shortcut in interelectrode region differs from the shortcuts above electrodes in several ways, mainly that (i) it appears in lower part of interelectrode region, (ii) one of the plasma to electrode contact points can be affected too, and (iii) it happens only near the voltage zero crossing and so it is effectively a channel reignition. As new glide ignitions also happen close to voltage zero crossings (note: with 50 Hz power supply this can be true only for gliding frequencies below 100 Hz; if the gliding frequency would be higher, the extinguishing necessarily happens also at non-zero voltage), this low shortcut can resemble the new glide ignition, however during shortcut at least one plasma to electrode contact point maintains its position and the discharge continues to propagate. The summary of the three principal events leading to the shortening of plasma channel, as observed during our experiments, is presented in table 1.

3.2. Maximum height and gliding frequency at normal gravity

The figures 3 and 4 are very useful to study the evolution during one glide period, but they lack statistical value and although they include the information about maximum reached height h_{max} before quenching of the discharge, they are not convenient for further discussion of h_{max}. Figure 8
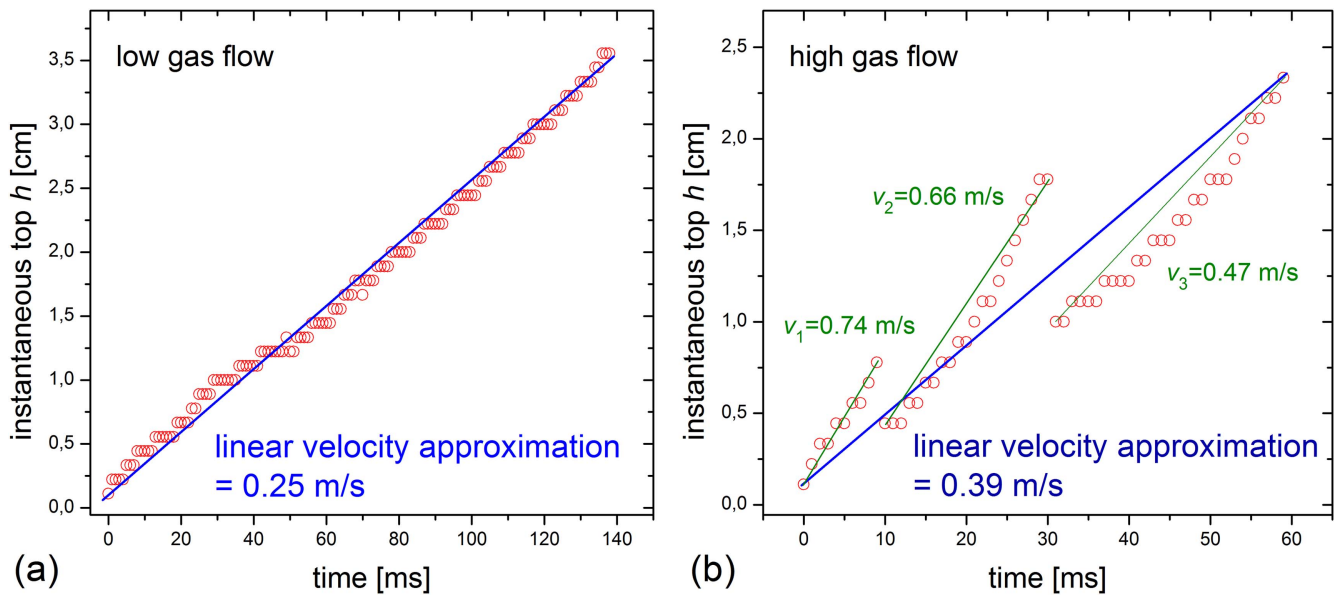
Figure 6. Temporal evolution of instantaneous top for one full glide of gliding arc in argon at 100 V primary voltage in two different flow rate conditions: (a) low gas flow rate = 280 sccm, (b) high gas flow rate = 1000 sccm.
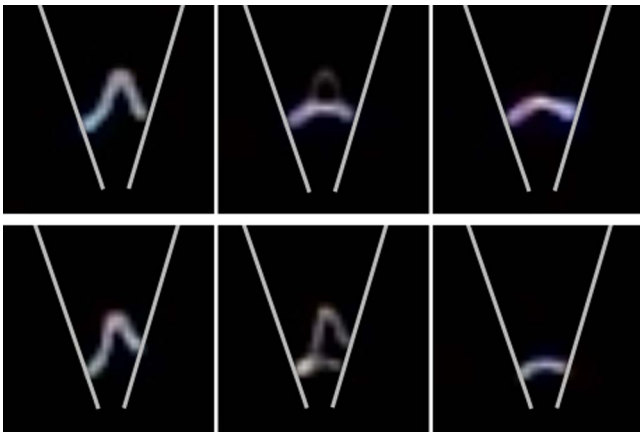

Figure 7. Two independent examples of shortcut events in the interelectrode region. The delay between successive video frames is 1 ms. Descent of one of the plasma-electrode contact points can be seen in lower set of images as well. Experimental conditions: argon, 1000 sccm, 100 V primary voltage, 1*g*.

directly shows the dependency of average h_{max} and gliding frequency on the primary voltage for the four noble gases at the same experimental conditions as in figure 4.

The average maximum height h_{max} shows the same general trend for all four gases—it always increases with voltage, as a higher voltage enables sustaining of a longer plasma channel, thus higher h_{max}. However, while the growth of average h_{max} with voltage is stable for helium and krypton gliding arcs, in neon and argon it exhibits a sudden transition to higher values. The voltages, at which this transition occurs, are different for neon and argon, as are the corresponding values of average h_{max}. One may speculate that similar transition regions exist also for helium and krypton, but are out of hereby examined range.

In figure 8 on the right, gliding frequency is presented as a function of primary voltage too. The transition regions are

slightly less distinguishable than for h_{max}, but as the gliding frequency effectively combines information of h_{max} and average speed of the plasma channel movement, some other additional information can be deduced. The gliding frequency seems to be the more sensitive parameter to changes in primary voltage than h_{max}, at least for the voltages resulting in low h_{max}. The best example of this is a trend in helium, where h_{max} is almost constant while the gliding frequency undergoes major changes, indicating significant decelerating of plasma channel at higher voltages. This is consistent with the discussion of instantaneous data in figure 4.

Interestingly, there is no clear dependence of gliding frequency (or average h_{max}) on atomic mass for the rest of noble gases under studied conditions. We can even see in figure 8 the crossing of argon and neon curves. The lowest gliding frequencies were measured for the discharge in argon at two highest voltages and for krypton at all voltages. The discharge channel at these conditions was reaching the highest and thus had to travel the longest distance, which resulted in the low gliding frequency. However, the gliding frequencies of discharge in neon (and helium) at highest voltages were also comparably low, although the average h_{max} reached by discharge in neon was less than a half of those in argon or krypton. The gliding frequency of discharge in helium was the highest of all gases, mainly because of higher gas flow rate that was necessary to induce gliding motion in this noble gas.

To study the influence of a gas flow, the h_{max} and gliding frequency dependence on primary voltage was measured again, now for 3 different gas flow rates, see figure 9. Argon was chosen as working gas for this type of experiment, as it underwent the most pronounced changes in previous overview experiment. The flow rates varied by 250 sccm below and above the already presented value of 400 sccm. The results revealed two main facts: (i) the sigmoid trend in

Table 1. Qualitative overview of principal types of events leading to shortening of the plasma channel.

	New glide ignition	Low shortcut	High shortcut
Discharge characteristics	No special conditions	High gas flow	Reaching high above electrodes
Occurrence position	Disrupts at maximum height, ignites at minimum bottom	Lower interelectrode region	Region above electrodes
Instantaneous top	Significant decrease	Minor decrease	Decrease
Instantaneous bottom	Significant decrease	Possible minor decrease	No change
Voltage phase	Zero crossing	Zero crossing	Any phase
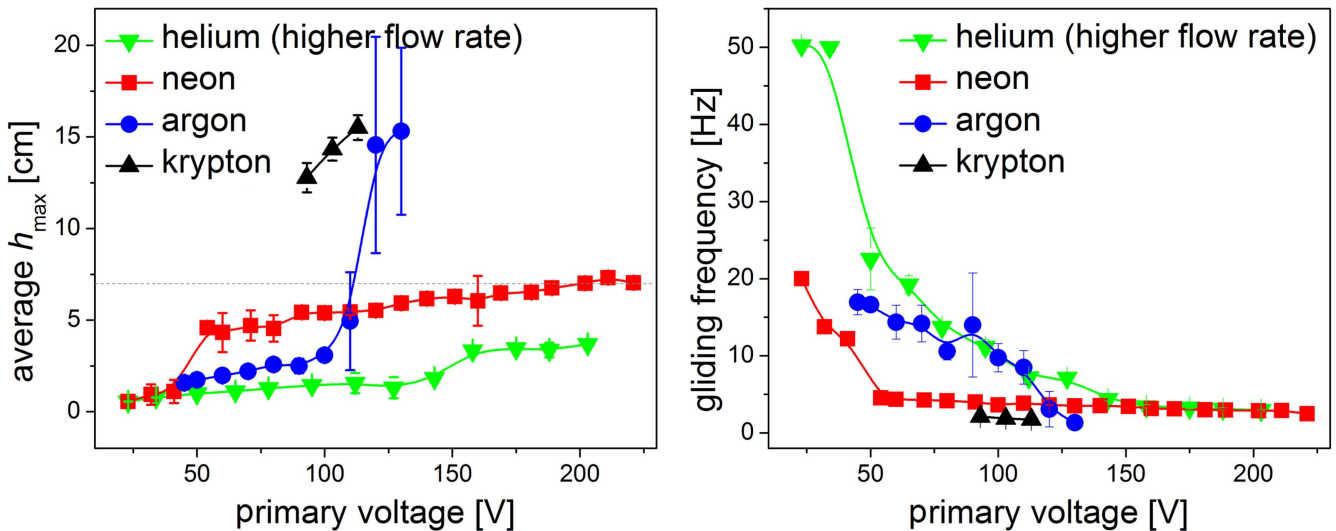
Figure 8. Average maximum height h_{max} and gliding frequency of gliding arc in four noble gases as a function of primary voltage at the same experimental conditions as in figure 4. Grey dashed line in left graph marks the upper border of the interelectrode region.

average h_{max} observed in previous figures—steadily growing h_{max}, until the sharp increase at transition region, followed by further minor growth—is present for all three flow rates, but (ii) it is steeper and shifted towards higher voltages for higher flow rates. It means, that the higher the gas flow, the higher voltage is needed to maintain the same average h_{max}. The high gas flow results in higher energy losses in the plasma channel [19], which have to be compensated by increased voltage and thus increased supplied power. The gliding frequency in figure 9 again shows more detail for lower voltages. Even though the average h_{max} for low voltages was essentially the same for all three gas flows, the frequency was several times higher for high flow rate, indicating very fast movement of plasma channel.

To further examine the transition region, of which the position depends on both the gas flow rate and the voltage (and on other parameters such as gas type, conceivably also the gravity, etc), the average h_{max} and gliding frequency of discharge in argon are shown in figure 10 as functions of the flow rate, now for constant primary voltage of 100 V. It can be seen that the average h_{max} decreases rapidly and stabilises at almost constant value for higher flow rates while the gliding frequency increases linearly and then roughly stabilises as well. However, the flow rates, at which this stabilisation occurs, are notably different for the two parameters, so for middle range of flow rates the gliding frequency still

increases significantly, even though the average h_{max} already remains constant. While the rapid decrease (grey box in figure 10) of average h_{max} seems to begin from the lowest flow rates, there is a lower limit of gas flow, under which the gliding ceases entirely.

3.2.1. Maximum height distribution at normal gravity conditions. In all presented graphs of average h_{max} (figures 8–10), the error bars were also included. While for lower heights the standard deviations were so small that the error bars are practically unnoticeable, for higher positions they were more prominent and the most outstanding they were for the transition region in-between. In figure 11, the instantaneous glide data (top and bottom) for three lowest gas flows from figure 10 (i.e. the grey box) represent this behaviour well. The distribution of h_{max} is markedly different for these 3 flow rates. One observes (i) low height stable region (here at 280 sccm), (ii) transition (or unstable) region (here at 190 sccm) and (iii) upper height stable region (here at 90 sccm). It can be seen, that for 90 and 280 sccm (the two stable regimes), each individual glide extinguishes at approximately the same h_{max}, just as expected on grounds of small error bars in figure 10 for corresponding data points. However, the case of intermediate flow rate of 190 sccm shows that even though the average value of h_{max} was slightly above 8 cm, in reality the individual gliding arcs reached
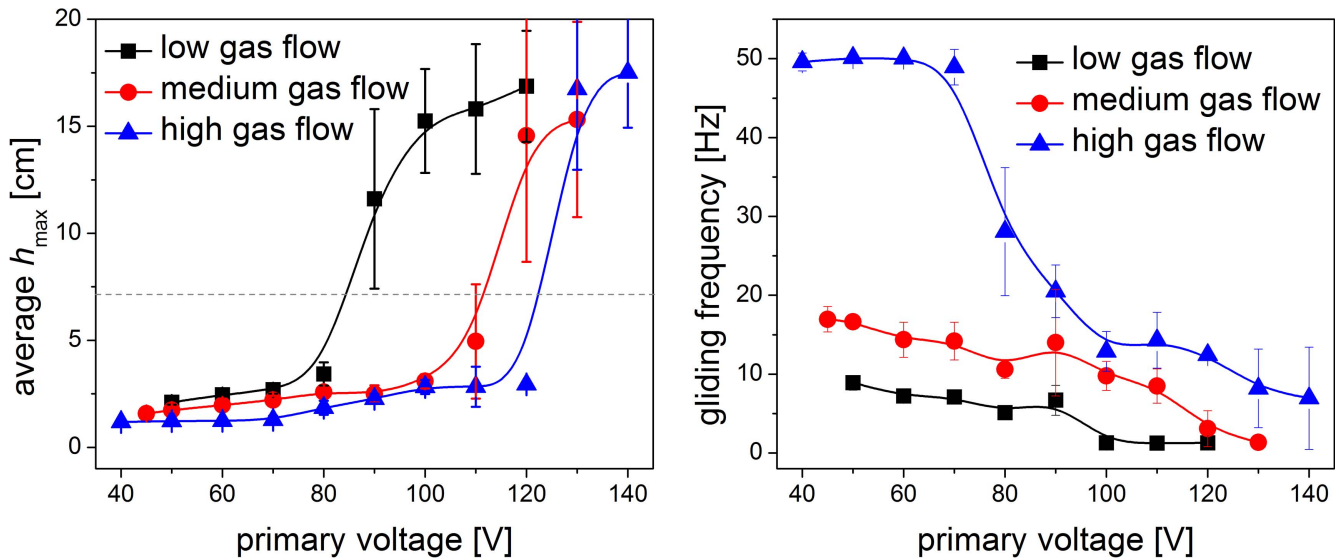
Figure 9. Average maximum height h_{max} and gliding frequency of gliding arc in argon at several flow rates (150, 400 and 650 sccm) and 1*g* gravity level as a function of primary voltage. Grey dashed line in left graph marks the upper border of the interelectrode region.
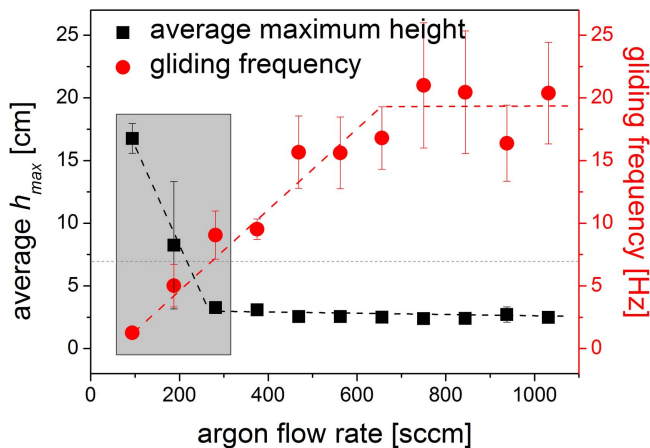

Figure 10. Average maximum height (black squares) and gliding frequency (red circles) of gliding arc in argon for 100 V primary voltage and 1*g* gravity level as a function of flow rate. Grey dashed line marks the upper border of the interelectrode region. Grey box marks the region of rapid h_{max} decrease, discussed in section 3.2.1.

either much higher or much lower. Interestingly, most of them were reaching either the h_{max} values of lower or upper stable region. The h_{max} in unstable transition regions seems to be oscillating between these two stable values and the steep, but continuous, drop (in figure 10) or rise (in figures 8 and 9) of average h_{max} is in fact just the gradual shift in the probability of occurrence of these two values.

Several more features can be noticed in figure 11. For 90 sccm flow rate, many individual glides are disrupted by shortcut events in the region above the electrodes (one example is marked by grey triangle), just like described in section 3.1. Further it can be seen that the higher the channel ascended, the bigger was the vertical distance between its instantaneous bottom and instantaneous top. This was always the case when the gliding arc reached above the interelectrode

region, as plasma-electrode contact points, here corresponding to the instantaneous bottom, can not move above the electrode top edge (causing horizontal parts of blue curves, one example is marked by grey circle). Smaller and more gradual separation of the instantaneous top and bottom sometimes occurred also in the interelectrode region, when the movement of plasma channel on electrodes slowed down (one example is marked by grey rectangle). The reason of this is probably the discontinuous movement of the plasma-electrode contact points, which rather 'jump' between local irregularities of the electrode surface. The plasma channel tends to 'stick' to the little bumps on the electrode edge surface, where local electric field is intensified. Just when the upwards forces overcome the advantages of this location, the contact point moves higher to another such one. This can cause the relatively slower movement of the plasma channel on the electrodes than in the central, unobstructed part of the plasma channel, resulting in different speed in instantaneous bottom and top. However, the contact point movement over the electrode roughness is a random process and the slowed movement is not always observable and even when it is, it's magnitude differs as well.

3.3. Maximum height and gliding frequency in hypergravity

In figure 12, more results obtained in hypergravity conditions are shown. Krypton was chosen as a working gas here, because the hypergravity had more pronounced influence on the discharge in krypton than in other gases, as is visible for example in figure 3 (the biggest decrease in maximum height). The effects of increased gravity on gliding arc are presented for three krypton gas flow rates (the same flow rates as in figure 9). The basic trend of increasing gravity influence is similar to that of increasing flow rate and opposite to that of increasing voltage at 1*g* conditions. It increases the gliding frequency and decreases the average h_{max}. The transition
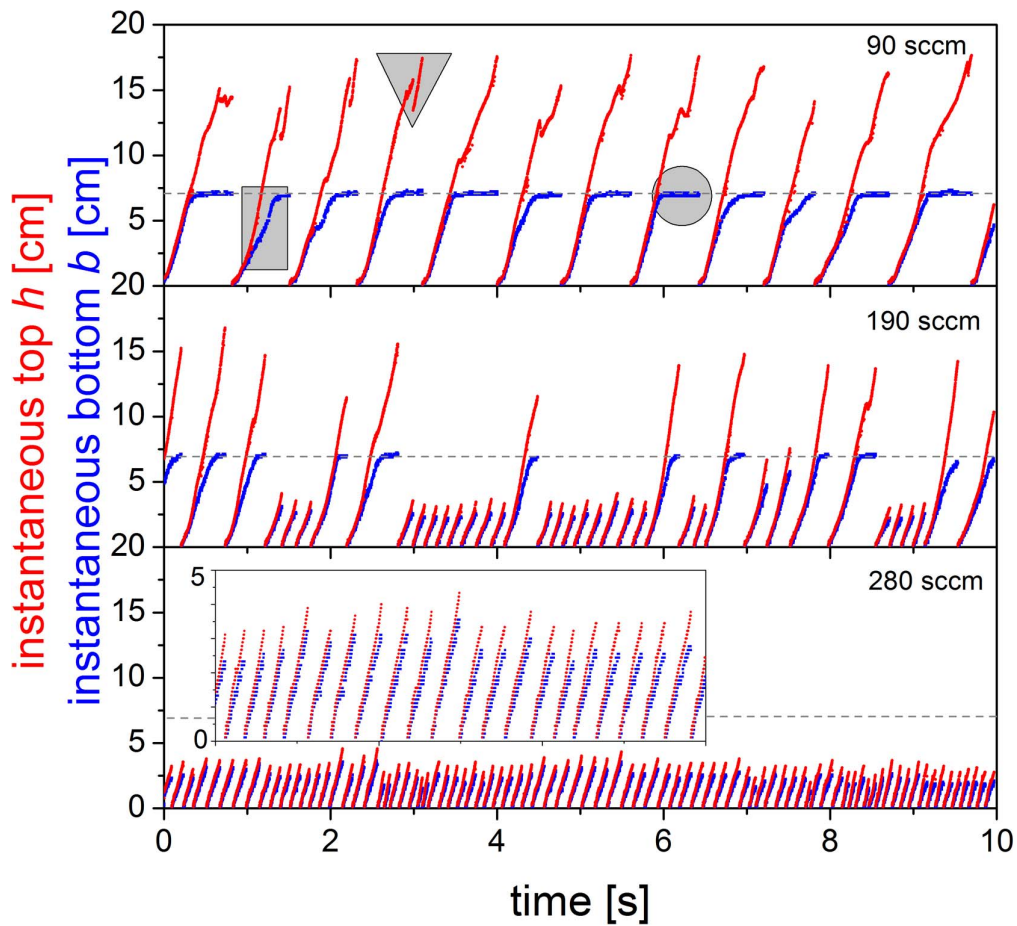
Figure 11. Continuous record (10 s) of instantaneous top and instantaneous bottom of gliding arc in argon. In the plot corresponding to 280 sccm, a magnified section of 3 s long interval is shown too. Grey dashed lines mark the upper border of the interelectrode region. Grey circle, rectangle and triangle mark the features discussed in the text.
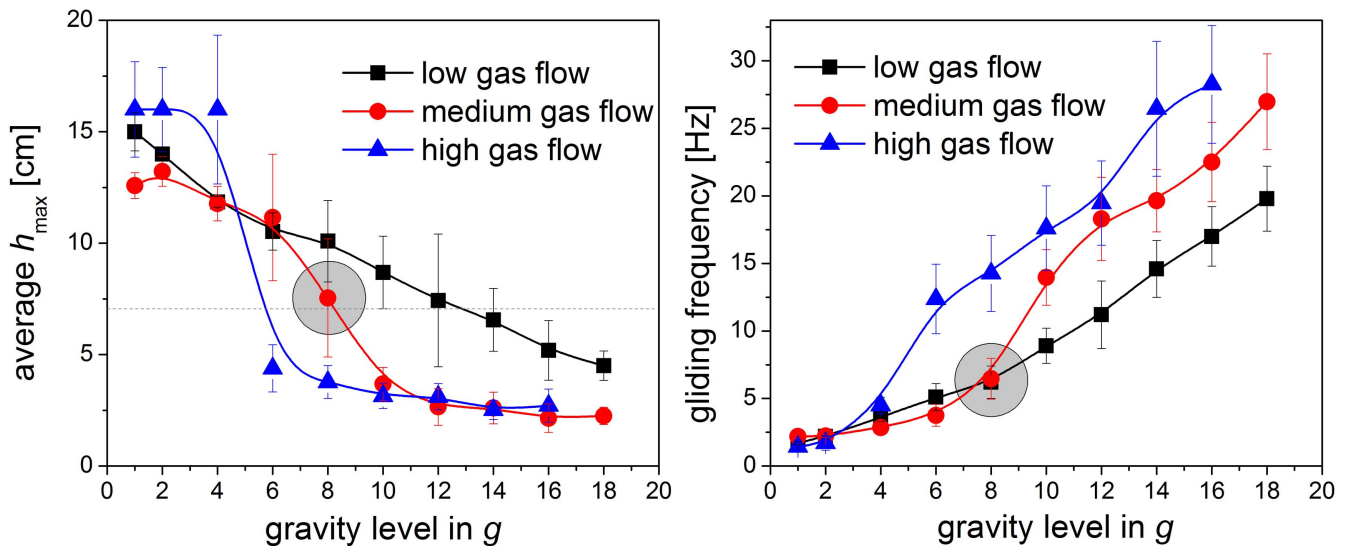

Figure 12. Average maximum height h_{max} and gliding frequency of gliding arc in krypton at several flow rates (same as in figure 9: 150, 400 and 650 sccm) and 100 V primary voltage as a function of gravity level. Grey dashed line in left graph marks the upper border of the interelectrode region. Grey circle marks a datapoint discussed in section 3.3.1.
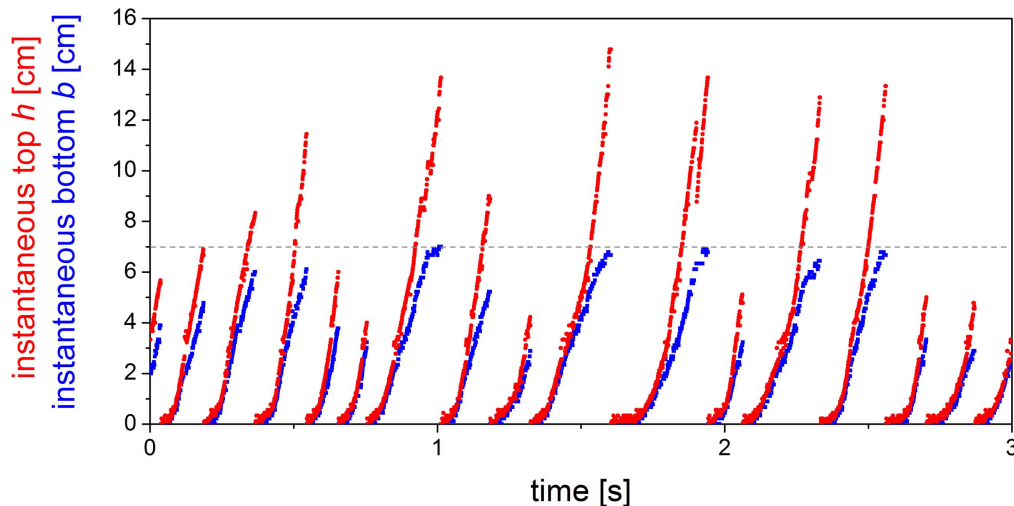
Figure 13. Continuous record (3 s) of instantaneous top and instantaneous bottom of the gliding arc in krypton in the transition region (at $8g$ and medium flow rate). Grey dashed line marks the upper border of the interelectrode region.

region is again present, but its significance varies among the three flow rates. The steep decrease in average h_{max} is the most pronounced for high gas flow rate. For medium gas flow rate it becomes less visible, yet still observable and for the lowest gas flow rate the decrease in average h_{max} is gradual and the transition region can be distinguished only by the largest error bar at $12g$. Importantly, the graph also shows that increasing the gas flow, the transition region shifts to lower g-levels, confirming the joint influence of the gas flow and buoyant forces on plasma channel movement.

3.3.1. Maximum height distribution in hypergravity. Similarly to figure 11, figure 13 also presents the instantaneous glide data, but now under hypergravity conditions. It shows the evolution of gliding motion for selected transition region data point in figure 12 (medium gas flow, $8g$ hypergravity, marked by the grey circle). Unlike before, there are not two (upper and lower) stable values of maximum height that could be distinguished. The increase in average h_{max} seems to be no longer a steep jump, as it was at $1g$, it appears more gradual in hypergravity and various maximum heights are represented.

3.4. Gas flow rate and hypergravity effects—similarities and differences

The main forces that drive the plasma channel upwards are the drag of gas flowing in the direction of gliding and the gravity dependent buoyant force acting on a heated plasma channel. In our experiment, these forces always acted simultaneously and so the upward force could be increased both by increasing the flow rate and/or increasing the g-level. With a stronger resulting force, the channel moved upwards faster. However, the faster moving channel suffered from more massive losses [19] of internal energy and excited plasma particles. As the losses increased, the power supply was not able to sustain the plasma channel over certain length and thus the maximum height necessarily decreased.

At low gas flow rate and/or low gravity, the forces that maintain the gliding motion became weaker and so the gliding was slower. As the movement was slower and steadier, the energy and particle losses got smaller and more remaining excited particles helped to form the plasma, reducing the power requirements for further prolonging and sustaining of the plasma channel. The example of gliding arc appearance at $1g$ and low gas flow conditions can be seen in figure 14, upper row.

However, there is a substantial difference between the two forces, as the gas flow introduced through a single bottom nozzle leads to strongly non-homogeneous drag force while the hypergravity field is nearly homogeneous over the discharge space (lateral and vertical gradients in LDC gondola cause differences in order of tenths of g which do not influence the experiment significantly). Some of the resulting differences in gliding arc appearance can be noticed on long exposure photographs in figure 14. The middle set of photographs represents the gliding arc at high gas flow conditions, while the lower set of photographs was taken during hypergravity experiments from inside the centrifuge gondola at $18g$. At both high gas flow and high gravity conditions, the strong upwards force caused high gliding frequency (in comparison with the upper row of photographs), so each of these long-exposure photographs comprises of many individual glides overlaying each other. Loss of temporal resolution makes the following of single filament difficult but it enables the image to carry the additional statistical information.

The above-mentioned difference in gravity field and gas flow velocity field leads to different shapes of the plasma region. In the middle row of photographs, the high gas flow in the axis of the nozzle results in a turbulent flow and plasma channel deformation. This gas drag induced deformation is more evident in the lower parts of interelectrode region, where the flux of gas is not yet dispersed.

As the thermal buoyancy force is spread over the whole plasma channel, the photographs in the lower row do not exhibit the central ridge. However, the plasma channel seems
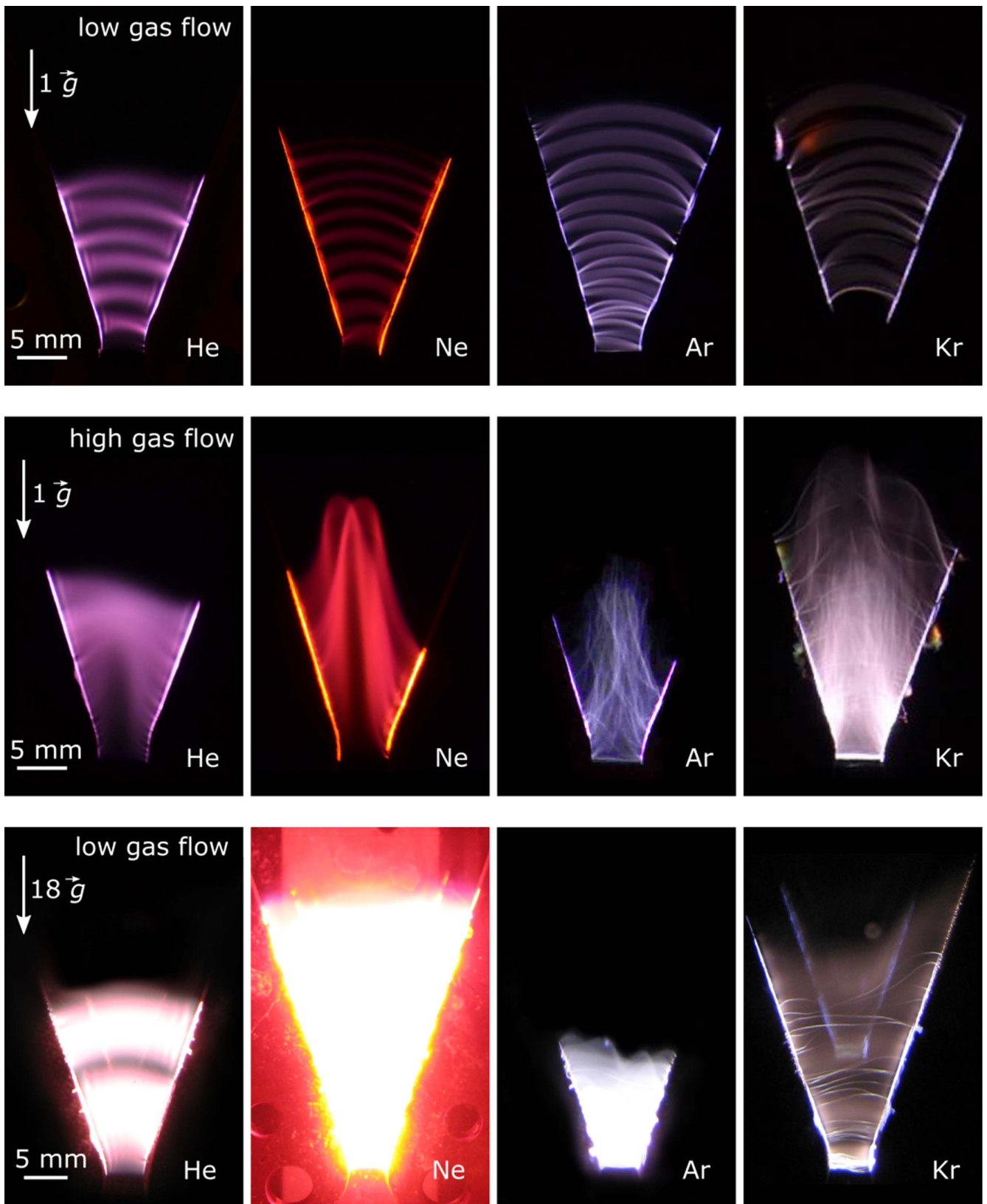
Figure 14. Long exposure photographs of gliding arc in four noble gases (He, Ne, Ar, Kr). Upper row: 1*g* gravity level, low gas flow. Middle row: 1*g* gravity level, high gas flow (1 slm higher). Lower row: 18*g* hypergravity level, low gas flow. The voltage and exposure time of photographs might differ in individual photographs and they are not important for discussion in this article. For broader set of conditions, more images can be found in [37]. Reproduced from [37]. © IOP Publishing Ltd. All rights reserved.

to be subjected to a random warping, forming small undulations. Overlaying minor irregularities can even mask the arc-like shape beneath. In a homogeneous gravity field, the buoyancy inhomogeneities leading to the channel warping can be caused by the local temperature variations in plasma channel. While these temperature deviations might not be significant enough to cause a visible plasma channel deformation under normal gravity, their influence becomes intensified at higher g-levels, where the sufficiently uneven forces acting on colder and hotter sections of the plasma channel result in its deformation.

This difference in character of both forces can also explain the presence/absence of well separated h_{max} values in transition region, observed only for regimes dominated by the gas flow. Gas drag affects every plasma channel approximately the same and its effect is not very sensitive to local variation in temperature. As a result, every channel is bended in a similar way. As the gas drag is concentrated in the lower parts of the inter-electrode region, high gliding speed and therefore high losses make the channel susceptible to quenching there. If any individual plasma channel happens to escape this turbulent region, the channel then can expand to its maximum elongation almost as in the case of low gas flow. The result is that observed h_{max} values fall into two separate sets—(i) either in lower, turbulent region or (ii) region corresponding to full extension of the channel in the calm area above the electrodes.

In contrast, the hypergravity is spatially homogenous, but its warping effects depend on local temperature variations. As a result, each channel is developing differently, i.e. randomly. High particle and heat losses due to high gliding speeds make the channel susceptible to quenching as well, but due to randomness of each channel, the h_{max} distribution is much wider.

4. Conclusion

In this work, AC gliding arc discharge was studied under a wide range of conditions by varying the type of gas and the flow rate, the supplied voltage and even the artificial gravity level. The focus of the investigation was on the characteristics of plasma channel upwards movement originating from the gravity dependent buoyant force and the flow rate dependent gas drag.

Detailed study of instantaneous position of moving plasma channel during one glide revealed that peculiarities of residual ionisation in plasma channel wake can affect the plasma channel motion. At certain conditions the nonlinear, sometimes even non-monotonous glides were observed. Three types of plasma channel shortening events, distinguished by vertical position and voltage phase at occurrence, were identified.

A quasi-periodic character of the gliding arc discharge encourages to complement the individual glide data by the statistical approach over many glides. The averaged maximum height reached by plasma channel was found to follow conceptually similar dependence on various parameters. The maximum height distribution in transition region is though

significantly different in the gas flow and in the gravity dominated regimes. The long-exposure photographs showing the general appearance of the gliding arc plasma helped to link this behaviour in transition region to the differences in spatial distribution of the two forces acting on plasma channel.

References

[1] Raizer Y P 1991 *Gas Discharge Physics* (Berlin: Springer)
[2] Fauchais P and Vardelle A 1997 Thermal plasmas *IEEE Trans. Plasma Sci.* **25** 1258–80
[3] Jang J and Nishiyama H 2015 Discharge study of argon DC arc jet assisted by DBD plasma for metal surface treatment *IEEE Trans. Plasma Sci.* **43** 3688–94
[4] Dolle G 1995 The evolution of the electric arc furnace *Rev. Metall.-Cah. D Inf. Tech.* **92** 10–1
[5] Fridman A, Chirokov A and Gutsol A 2005 Non-thermal atmospheric pressure discharges *J. Phys. D: Appl. Phys.* **38** R1–24
[6] Machala Z, Marode E, Laux C O and Kruger C H 2004 DC glow discharges in atmospheric pressure air *J. Adv. Oxid. Technol.* **7** 133–7
[7] Andrade F J, Wetzel W C, Chan G C-Y, Webb M R, Gamez G, Ray S J and Hieftje G M 2006 A new, versatile, direct-current helium atmospheric-pressure glow discharge *J. Anal. At. Spectrom.* **21** 1175–84
[8] Staack D, Farouk B, Gutsol A and Fridman A 2005 Characterization of a dc atmospheric pressure normal glow discharge *Plasma Sources Sci. Technol.* **14** 700–11
[9] Arkhipenko V I, Kirillov A A, Safronau Y A, Simonchik L V and Zgirouski S M 2012 Plasma non-equilibrium of the DC normal glow discharges in atmospheric pressure atomic and molecular gases *Eur. Phys. J.* D **66** 252
[10] Staack D, Farouk B, Gutsol A and Fridman A 2008 DC normal glow discharges in atmospheric pressure atomic and molecular gases *Plasma Sources Sci. Technol.* **17** 025013
[11] Andre P *et al* 2001 Experimental study of discharge with liquid non-metallic (tap-water) electrodes in air at atmospheric pressure *J. Phys. D: Appl. Phys.* **34** 3456–65
[12] Becker K H *et al* 2010 Microplasmas: scientific challenges & technological opportunities *Eur. Phys. J.* D **60** 437–9
[13] Gibalov V I and Pietsch G J 2000 The development of dielectric barrier discharges in gas gaps and on surfaces *J. Phys. D: Appl. Phys.* **33** 2618–36
[14] Hoder T, Loffhagen D, Wilke C, Grosch H, Schafer J, Weltmann K-D and Brandenburg R 2011 Striated microdischarges in an asymmetric barrier discharge in argon at atmospheric pressure *Phys. Rev.* E **84** 046404
[15] Stark R H and Schoenbach K H 1999 Direct current glow discharges in atmospheric air *Appl. Phys. Lett.* **74** 3770

[16] Li X, Liu R, Jia P, Bao W and Shang Y 2013 Self-pulsing discharge of a plasma brush operated in atmospheric-pressure argon *Europhys. Lett.* **102** 55003

[17] Jiang W, Tang J, Wang Y, Zhao W and Duan Y 2014 Characterization of argon direct-current glow discharge with a longitudinal electric field applied at ambient air *Sci. Rep.* **4** 6323

[18] Zhang C, Shao T, Xu J, Ma H, Duan L, Ren C and Yan P 2012 A gliding discharge in open air sustained by high-voltage resonant ac power supply *IEEE Trans. Plasma Sci.* **40** 2843–9

[19] Fridman A A, Nester S, Kennedy L A, Saveliev A V and Mutaf-Yardimci O 1999 Gliding arc gas discharge *Prog. Energy Combust. Sci.* **25** 211–31

[20] Kuznetsova I V, Kalashnikov N Y, Gutsol A F, Fridman A A and Kennedy L A 2002 Effect of 'overshooting' in the transitional regimes of the low-current gliding arc discharge *J. Appl. Phys.* **92** 4231–7

[21] Diatczyk J, Komarzyniec G and Stryczewska H D 2011 Power consumption of gliding arc discharge plasma reactor *Int. J. Plasma Environ. Sci. Technol.* **5** 12–6

[22] Zhu J, Sun Z, Li Z, Ehm A, Alden M, Salewski M, Leipold F and Kusano Y 2014 Dynamics, OH distribution and UV emission of a gliding arc at various flow-rates investigated by optical measurements *J. Phys. D: Appl. Phys.* **47** 295203

[23] Mutaf-Yardimci O, Saveliev A V, Fridman A A and Kennedy L A 2000 Thermal and nonthermal regimes of gliding arc discharge in air flow *J. Appl. Phys.* **87** 1632–41

[24] Kolev S and Bogaerts A 2015 Similarities and differences between gliding glow and gliding arc discharges *Plasma Sources Sci. Technol.* **24** 065023

[25] Pellerin S, Cormier J-M, Richard F, Musiol K and Chapelle J 1999 Determination of the electrical parameters of a bi-dimensional d.c. Glidarc *J. Phys. D: Appl. Phys.* **32** 891–7

[26] Korolev Y D, Frants O B, Geyman V G, Landl N V and Kasyanov V S 2011 Low-current 'gliding arc' in an air flow *IEEE Trans. Plasma Sci.* **39** 3319–25

[27] Korolev Y D, Frants O B, Landl N V, Bolotov A V and Nekhoroshev V O 2014 Features of a near-cathode region in a gliding arc discharge in air flow *Plasma Sources Sci. Technol.* **23** 054016

[28] Kolev S and Bogaerts A 2015 A 2D model for a gliding arc discharge *Plasma Sources Sci. Technol.* **24** 015025

[29] Czernichowski A, Nassar H, Ranaivosoloarimanana A, Fridman A A, Simek M, Musiol K, Pawelec E and Dittrichova L 1996 Spectral and electrical diagnostics of gliding arc *Acta Phys. Pol.* A **89** 595–603

[30] Kalra C S *et al* 2005 Gliding arc in tornado using reverse vortex flow *Rev. Sci. Instrum.* **76** 025110

[31] Balcon N, Benard N, Braud P, Mizuno A, Touchard G and Moreau E 2008 Prospects of airflow control by a gliding arc in a static magnetic field *J. Phys. D: Appl. Phys.* **41** 205204

[32] Zhu J, Ehn A, Gao J, Alden M, Li Z, Hurtig T, Larsson A and Kusano Y 2015 Effects of gliding arc discharge penetrating a premixed flame *European Combustion Meeting*

[33] Czernichowski A 1994 Gliding arc, applications to engineering and environment control *Pure Appl. Chem.* **66** 1301–10

[34] Kalra C S, Gutsol A F and Fridman A A 2005 Gliding arc discharges as a source of intermediate plasma for methane partial oxidation *IEEE Trans. Plasma Sci.* **33** 32–41

[35] Tu X and Whitehead J C 2014 Plasma dry reforming of methane in an atmospheric pressure AC gliding arc discharge: co-generation of syngas and carbon nanomaterials *Int. J. Hydrogen Energy* **39** 9659–69

[36] Mitsugi F, Ohshima T, Kawasaki H, Kawasaki T, Aoqui S-I, Baba T and Kinouchi S 2014 Gas flow dependence on dynamic behaviour of serpentine plasma in gliding arc discharge system *IEEE Trans. Plasma Sci.* **42** 3681–6

[37] Potočňáková L, Šperka J, Zikán P, van Loon J J, Beckers J and Kudrle V 2015 Gravity effects on a gliding arc in four noble gases: from normal to hypergravity *Plasma Sources Sci. Technol.* **24** 022002

[38] Šperka J, Souček P, Van Loon J J, Dowson A, Schwarz C, Krause J, Kroesen G and Kudrle V 2013 Hypergravity effects on glide arc plasma *Eur. Phys. J.* D **67** 261

[39] Šperka J, Souček P, Van Loon J J, Dowson A, Schwarz C, Krause J, Butenko Y, Kroesen G and Kudrle V 2014 Hypergravity synthesis of graphitic carbon nanomaterial in glide arc plasma *Mater. Res. Bull.* **54** 61–5

[40] Potočňáková L, Šperka J, Zikán P, van Loon J J, Beckers J and Kudrle V 2014 Gliding arc in noble gases under normal and hypergravity conditions *IEEE Trans. Plasma Sci.* **42** 2724–5

[41] van Loon J J W A, Krause J, Cunha H, Goncalves J, Almeida H and Schiller P 2008 The large diameter centrifuge for life and physical sciences and technology *Proc. Life in Space for Life on Earth Symp. (Angers, France, 22–27 June 2008)* ESA SP-663

[42] Wolfram Research Inc. 2014 Mathematica, Version 10.0, Champaign, IL

[43] Pejovic M M, Ristic G S and Karamarkovic J P 2002 Electrical breakdown in low pressure gases *J. Phys. D: Appl. Phys.* **35** R91–103

[44] Kudrle V, LeDuc E and Fitaire M 1999 Breakdown delay times and memory effects in helium at low pressure *J. Phys. D: Appl. Phys.* **32** 2049–55

[45] Petrovic Z L, Markovic V L, Pejovic M M and Gocic S R 2001 Memory effects in the afterglow: open questions on long-lived species and the role of surface processes *J. Phys. D: Appl. Phys.* **34** 1756–68